

ON HIGH-ORDER POLYNOMIAL HEAT-BALANCE INTEGRAL IMPLEMENTATIONS

by

Alastair S. WOOD, Farida MOSALLY, and Abdul AL-FHAID

Original scientific paper
UDC: 536.255:519.161
BIBLID: 0354-9836, 13 (2009), 2, 11-25
DOI: 10.2298/TSCI0902011W

This article reconsiders aspects of the analysis conventionally used to establish accuracy, performance and limitations of the heat balance integral method: theoretical and practical rates of convergence are confirmed for a familiar piecewise heat-balance integral based upon mesh refinement, and the use of boundary conditions is discussed with respect to fixed and moving boundaries.

Alternates to mesh refinement are increased order of approximation or non-polynomial approximants. Here a physically intuitive high-order polynomial heat balance integral formulation is described that exhibits high accuracy, rapid convergence, and desirable qualitative solution properties. The simple approach combines a global approximant of prescribed degree with spatial sub-division of the solution domain. As a variational-type method, it can be argued that heat-balance integral is simply "one amongst many". The approach is compared with several established variational formulations and performance is additionally assessed in terms of "smoothness".

Key words: *heat balance integral, high-order polynomial approximants*

Introduction

The semi-analytical heat-balance integral method (HBIM) proposed by Goodman [1] provides approximate functional solutions to transport phenomena governed by partial differential equations. Spatial boundary conditions are satisfied by the chosen approximant, together with an integral (weak) form of the governing conservation equation(s). The resilience of the method over the past 50 years to the emergence of increasingly sophisticated numerical methodologies and exponentially increasing computer power is a testament to the soundness of its inherent simplicity, based as it is upon the fundamental conservation laws of the problem to be tackled (which makes it appealing to scientists and engineers alike) together with simple underlying approximants that are easily manipulated and enumerated. These two principles make it readily applicable to a wide range of problems, in particular those containing non-linear contributions that comprise the more realistic descriptions of industrial process models.

Goodman's [1] approach was to construct quadratic temperature profiles for transient one-dimensional heat transfer, with and without phase change, later successfully applied to several two-phase melting problems by Goodman *et al.* [2]. In 1964 Goodman published his extensive survey of integral methods applied to heat transfer problems, of which the HBIM is one [3].

Since Goodman's proposal [1] many papers have been published that describe improvements to the accuracy of the original method, in addition to numerous descriptions of ap-

plications of the method. Early papers described modifications to the basic quadratic profile, including moderate increases in the degree of the approximant, and from the mid 1970s the focus shifted to spatial and temperature sub-division coupled with low-order piecewise approximants.

Goodman's (first) refinement of the HBIM developed cubic and quartic polynomial profiles for transient pure heat conduction in one-dimension [4]. Additional constants appearing in the higher-order profiles were evaluated by satisfying extra derived conditions (*without* obvious physical meaning) at a specified penetration depth beyond which no heat transfer took place. Hills [5] generalised the integral method by characterising the solidification process by two parameters (thickness of the solidified layer and temperature of the outer surface) as opposed to the conventional single-parameter characterisation using thickness alone. The approach, validated against experimental evidence [6], was very effective at dealing with a wide range of cooling conditions. Langford [7] gave an accuracy criterion for the HBIM using higher-order approximants based upon satisfying a number of derived conditions at the phase-change boundary.

Noble [8] suggested a combination of spatial sub-division and low-order piecewise approximants as an alternative refinement of the HBIM. Bell [9, 10] discussed spatial sub-division for both plane and radial geometries and in each case demonstrated the effectiveness of the solution using only a few sub-divisions and piecewise linear approximants, hard to better even to this day. The approach also circumvents the acknowledged sensitivity of the HBIM to the selected approximant. Bell [11] introduced the use of temperature sub-division and the modification was successfully applied to the two-phase solidification problem of estimating the penetration depth of frost [12]. Bell *et al.* [13] presented an analysis that established the formal convergence of the HBIM, using the earlier refinement [9], to the analytic solution for pure heat conduction in a semi-infinite medium. This was later generalised to include phase-change by Mosally *et al.* [14].

This short review focussed upon implementation, and neglected a myriad of reports on application areas of the HBIM, the extension from Cartesian coordinates to both cylindrical and spherical coordinates typified by, amongst others, Caldwell [15-18] and Bell [10], and the use of non-polynomial approximants. In this vein, this paper discusses the use of polynomial approximants of arbitrary order within the context of the HBIM. A simple technique, in the spirit of the original concept, is proposed for generating the additional equations (*with* physical meaning) required to evaluate the extra coefficients appearing in higher-order approximants. A highly accurate global approximation is obtained with excellent convergence properties. The approaches of Goodman [4] and Langford [7] would be very complicated, and not unambiguous, to apply to an approximant of arbitrary degree.

Model problem

To place the present proposal, the popular piecewise refinement [13] is implemented together with several familiar variational methods. Features of the method are demonstrated by application to a dimensionless problem describing single-phase melting of ice:

$$\frac{\partial U}{\partial t} - \frac{\partial^2 U}{\partial x^2}, \quad 0 \leq x \leq s(t), \quad t \geq 0 \quad (1)$$

$$U(0, t) = 1, \quad t > 0 \quad (2)$$

$$U(x, t) = 0, \quad x = s(t), \quad t > 0 \quad (3)$$

$$U(x, 0) = 0, \quad x \geq 0 \tag{4}$$

$$\frac{\partial U}{\partial x} = \beta \frac{ds}{dt}, \quad x = s(t), \quad t > 0 \tag{5}$$

Equation (1) describes heat flow in the liquid region, eqs. (2) and (3) set the fixed boundary ($x = 0$) and moving melt front [$x = s(t)$] temperatures, eq. (4) sets the initial temperature, the Stefan condition (5) describes heat absorption at the melt front ($\beta = L/c(T_0 - T_m)$ is the ratio of latent to sensible heat). The exact solution to model (1)-(5) is:

$$U(x, t) = 1 - \frac{\operatorname{erf} \frac{x}{2\sqrt{t}}}{\operatorname{erf}(\alpha)}, \quad 0 \leq x \leq s(t), \quad t > 0 \tag{6}$$

$$s(t) = 2\alpha\sqrt{t}, \quad t > 0 \tag{7}$$

where α is the root of the equation $\pi^{1/2}\alpha\operatorname{erf}(\alpha) \exp\alpha^2 = \beta$. The model and its solution are easily related to a physical description by the variable changes $X = lx, \tau = l^2t/\kappa, T = T_m + (T_0 - T_m)U$, and $S = ls$.

Heat-balance integral method

For the model (1)-(5) the conventional piecewise linear HBIM [13] divides the domain $[0, s]$ into n sub-intervals of length s/n on which the temperature U is approximated by a piecewise linear profile:

$$v = v_{i-1} + \frac{n(x - x_{i-1})(v_i - v_{i-1})}{s}, \quad x_{i-1} \leq x \leq x_i, \quad i = 1, \dots, n \tag{8}$$

$v_i = U(x_i, t), v_0 = 1, v_n = 0$ and $x_i = is/n$. Generating a heat-balance integral on each sub-interval:

$$\int_{x_{i-1}}^{x_i} \frac{\partial U}{\partial t} dx = \frac{\partial U}{\partial x} \Big|_{x=x_i} - \frac{\partial U}{\partial x} \Big|_{x=x_{i-1}}, \quad i = 1, \dots, n \tag{9}$$

replacing U by the profile (8), with piecewise constant temperature gradient:

$$\frac{\partial v}{\partial x} \Big|_{x=x_i} = \frac{n(v_{i-1} - v_i)}{s}, \quad i = 0, \dots, n-1, \quad \frac{\partial v}{\partial x} \Big|_{x=x_n} = \beta \frac{ds}{dt} \tag{10}$$

yields a system of n ordinary differential equations for v_1, \dots, v_{n-1} and s :

$$s \frac{ds}{dt} = \frac{2n^2}{2i-1} \frac{v_{i-2} - 2v_{i-1} + v_i}{v_i - v_{i-1}}, \quad i = 0, 1, \dots, n-2 \tag{11}$$

$$s \frac{ds}{dt} = \frac{2n^2 v_{n-1}}{(2n-1)v_{n-1} - 2n\beta} \tag{12}$$

From eqs. (11) and (12), v_i can be expressed as a three-term recurrence relation:

$$v_i - v_{i-1} = (v_{i-2} - v_{i-1})f_i, \quad i = n-2, n-3, \dots, 1, 0 \tag{13}$$

where

$$f_i = \frac{n - \eta}{n - \eta - i + 1}, \quad \eta = \frac{1}{v_{n-1}} \tag{14}$$

Repeated application of eq. (13), with $v_0=1$, yields a polynomial equation for η :

$$1 - \frac{\eta}{n} - \frac{\eta^2}{n(n-1)} - \frac{\eta^3}{n(n-1)(n-2)} - \dots - \frac{\eta^{n-1}}{n(n-1)\dots(\eta-k)} = 0 \quad (15)$$

On solving eq. (15) for η , the approximate temperature profile is obtained from eqs. (13) and (14), and the melt front is found by solving eq. (12):

$$s = \frac{2n\sqrt{t}}{\sqrt{2n-2\eta-1}} - 2\alpha^*\sqrt{t}, \quad \alpha^* = \frac{n}{\sqrt{2n-2\eta-1}} \quad (16)$$

Figure 1(a) shows the spatial relative error for three successive refinements, plus the error of a high-accuracy solution obtained via Richardson's extrapolation. Figure 1(b) shows \log_{10} error, effectively the number of significant digits (obtained at little additional arithmetic cost). Extrapolation almost doubles the number of significant digits. However, what is evident is the wide range of accuracy across the spatial domain, changing by at least one order of magnitude for the basic solutions, and by two orders of magnitude in the extrapolated solution. This uneven distribution of accuracy is, perhaps, a less familiar feature of the HBIM, and is not particularly desirable.

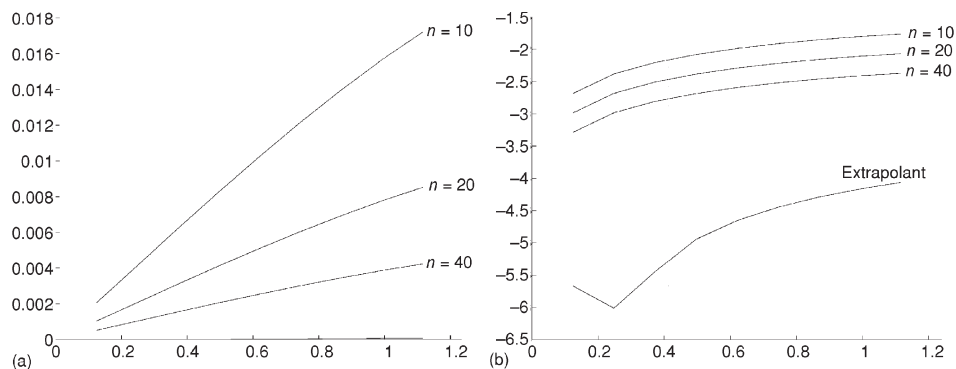


Figure 1. Spatial (relative) error in temperature for $n = 10, 20,$ and 40 sub-intervals
(a) error, (b) \log_{10} error

In the numerical frame work developed above, the moving boundary condition (5) is explicitly incorporated into the formulation. Due in part, perhaps, to the use of time-dependent constants in the approximants such as Goodman's [3]

$$v = a(x-s) + b(x-s)^2 \quad (17)$$

earlier authors have tended to use the derived moving-boundary condition:

$$\frac{\partial U}{\partial x} = \beta \frac{\partial^2 U}{\partial x^2}, \quad x = s(t), \quad t = 0 \quad (18)$$

based upon the governing differential equation being satisfied on the moving boundary. Strictly this is not true, and use of eq. (18) can lead to significant variation in solution accuracy [19], particularly as the Stefan constant β varies.

Table 1. Accuracy of boundary-condition combinations as a function of β ; A – best, B – average, C – worst [19]

Stefan	Eq.	HBI v/x	β interval				
			Min. >0	0.055	0.064	0.075	2/15
			Max. 0.055	0.064	0.075	2/15	
1	Eq. (5)	Eq. (5)	A	B	C	C	A
2	Eq. (5)	Eq. (18)	Fail				
3	Eq. (5)	Eq. (19)	A	B	C	C	A
4	Eq. (18)	Eq. (5)	B	A	A	B	B
5	Eq. (18)	Eq. (18)	C	C	B	A	C
6	Eq. (18)	Eq. (19)	C	C	B	A	C

Figures 2(a) and 2(b) show the variation in error of the melt front parameter estimates provided by the six boundary-condition pairs listed in tab. 1 (option 2 fails completely). The column "Stefan" identifies the equation used to drive the moving boundary, and the column "HBI" denotes the condition used to evaluate v/x at $x=s(t)$ in the HBI solution process. The most accurate option is dependent upon β and the final 5 columns of tab. 1 quantify the intervals. The conclusion of these observations is that naive implementation of the HBIM will not maximise its approximation potential.

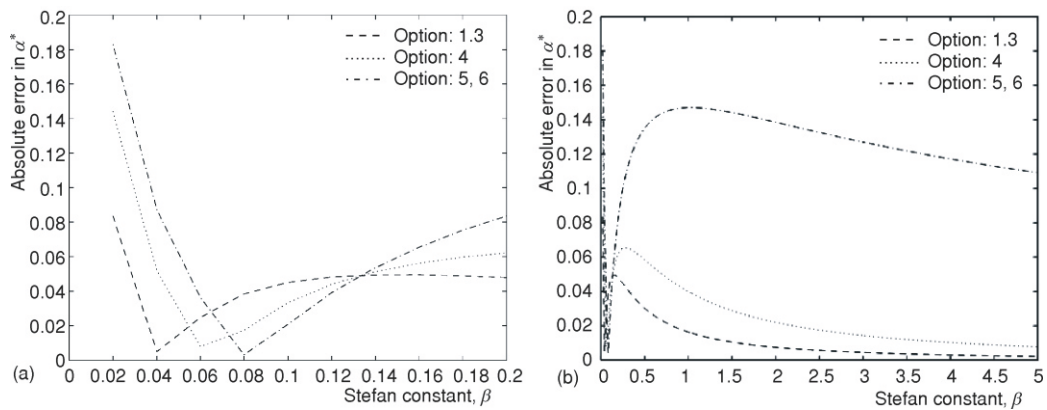


Figure 2. Error in melt front parameter α^* for boundary condition combinations [19]
 (a) small β , (b) large β

High-order polynomial approximations

Given the high accuracy but poor error distribution provided by mesh refinement of the HBI, here we seek high accuracy by 'order' with the additional goal of improving uniformity of error.

We seek a polynomial solution v of degree $N - 2$ to eqs. (1)-(5)

$$v(x, t) = \sum_{i=1}^N a_i \left(1 - \frac{x}{s}\right)^i, \quad 0 \leq x \leq s(t) \quad (19)$$

where a_1, \dots, a_N are constants to be determined, v satisfies the spatial condition (3), and enforcing the spatial conditions (2) and (5) requires:

$$\sum_{i=1}^N a_i = 1 \quad (20)$$

$$a_1 = \beta_s \frac{ds}{dt} \quad (21)$$

Equation (21) implies the familiar square-root behaviour for the motion of the phase-change boundary, $s(t) = (2a_1 t / \beta)^{1/2}$, and so $(a_1 / 2\beta)^{1/2}$ is an estimate to the melt front parameter α .

If $N = 2$ [1] then eq. (20), $a_1 + a_2 = 1$, is combined with the standard HBI of the partial differential equation (1):

$$\frac{\partial U}{\partial t} = \frac{\partial^2 U}{\partial x^2} \quad (22)$$

in which U is replaced by the approximant v . In this way the two coefficients $a_1 = 61^{1/2} - 7$ and $a_2 = 8 - 61^{1/2}$ are obtained, and:

$$v(x, t) = \left(1 - \frac{x}{s}\right)^{\sqrt{61} - 7} \left(8 - \sqrt{61}\right) + \left(1 - \frac{x}{s}\right)^{8 - \sqrt{61}}, \quad 0 \leq x \leq s(t) \quad (23)$$

Figure 3 provides a comparison of the exact and approximate solutions, eqs. (6) and (23), for $\beta = 1$. The temperature profiles – fig. 3(a) – and melt front histories – fig. 3(b) – exhibit the familiar close agreement.

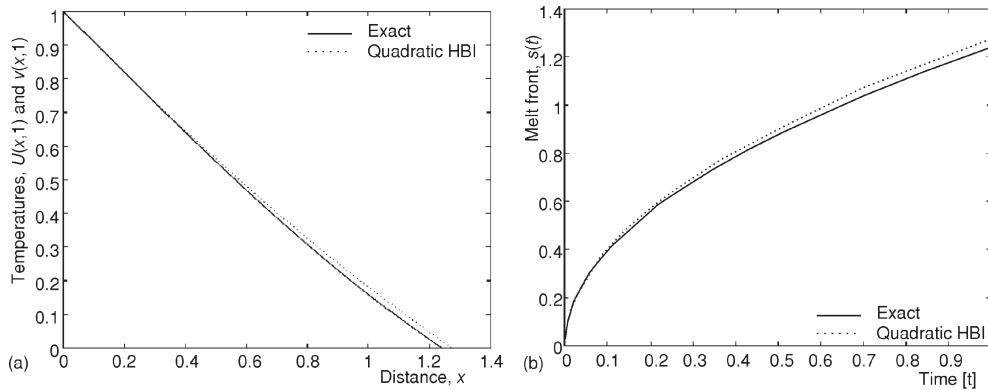


Figure 3. Exact and quadratic HBIM solutions to the model (1)-(5), $\beta = 1$, at $t = 1$
(a) temperature profile, (b) melt front history

Spatial sub-division

To generalise the standard HBI (22) for $N = 2$, and evaluate a_1, \dots, a_N , we sub-divide $[0, s]$ into $N - 1$ cells of size $s/(N - 1)$ and establish a HBI on each cell:

$$\frac{\partial U}{\partial t} = \frac{\partial^2 U}{\partial x^2} = \frac{\partial U}{\partial x} \Big|_{x_{j-1}}^{x_j}, \quad j = 1, \dots, N - 1 \quad (24)$$

where $x_j = js/(N - 1)$. The sub-division does not generate a piecewise approximant – eqs. (8) and (9) – but forces local energy balances for a global approximant on a set of sub-domains as opposed to a global balance across the entire domain $[0, s]$. As N increases so eq. (24) is a statement of an increasingly local (strong) heat-balance. On replacing U by the approximant (19), eq. (24) can be written in the form:

$$\sum_{i=1}^N a_i [a_i A_{mi} - B_{mi}] = 0, \quad m = 0, \dots, N - 2 \tag{25}$$

$$A_{mi} = \frac{(n - m)^i (im - n) - (n - m - 1)^i (im - i - n)}{n^{i-1} (i - 1)} \tag{26}$$

$$B_{mi} = \frac{i[(n - m)^{i-1} - (n - m - 1)^{i-1}]}{n^{i-1}}$$

where $(n = N - 1, m = j - 1)$

Equations (20) and (25) describe a system of N non-linear equations for $a = [a_1, \dots, a_N]^T$ of the form $f(a) = 0$. $f = [f_1 \dots f_N]^T$ denotes the functional form of the N equations:

$$f_1 = \sum_{i=1}^N a_i - 1$$

$$f_{m+2} = \sum_{i=1}^N a_i [a_i A_{mi} - B_{mi}], \quad m = 0, \dots, N - 2$$

readily solved by Newton’s method (see the section *Results and discussion*). If $N = 2$ ($m = 0$) this formulation recreates Goodman’s original quadratic [1]. However, in Goodman’s solution the a_i are functions of time whereas here they are independent of time due to the choice of basis in eq. (19).

Variational methods

The foregoing description resembles established variational solvers for PDEs. To highlight advantages of the proposed formulation, two familiar weighted-residual techniques are applied to eqs. (1)-(5): Galerkin (weights are approximant basis functions) and collocation. All three approaches shares the advantage that a functional is not required, which for time-dependent problems can be difficult to develop (e. g. Rayleigh-Ritz selects constants a_i to minimise a positive definite functional associated with the governing PDE).

Galerkin

The governing eq. (1) is multiplied by the weight function $(1 - x/s)^m$ and integrated over the spatial domain to generate $N - 1$ identities:

$$\int_0^s (1 - \frac{x}{s})^m \frac{\partial U}{\partial t} dx - \int_0^s (1 - \frac{x}{s})^m \frac{\partial^2 U}{\partial x^2} dx, \quad m = 0, \dots, N - 2 \tag{27}$$

This reduces to the conventional form (22) when $N = 2$ ($m = 0$). With increasing m more emphasis upon the evolving heat transfer process is given to the effect of the temperature profile “far” from the phase-change boundary (the basic HBIM formulation gives equal weight to all points in the domain $[0, s]$). Equations (27) and (20) may be used to determine a_1, \dots, a_N . On substituting the polynomial profile (19) into eq. (27), we obtain the algebraic system (25), where now:

$$A_{mi} = \frac{i}{(m-i)(m-i-1)}, \quad B_{mi} = \begin{cases} 0, & i=1 \\ \frac{i(i-1)}{m-i-1}, & i=2, \dots, n \end{cases} \quad (28)$$

Collocation

The residual $r = U_t - U_{xx}$ is set to zero at $N-1$ equi-spaced internal nodes $x_j = js/N$, $j = 1, \dots, N-1$, to define equations for a_1, \dots, a_N the boundary conditions on temperature are satisfied by the approximant (19). Replacing U by v in the residual and enforcing the $N-1$ nodal conditions $r[v(x_j)] = 0$ generates the system (25) with (note that $m = j-1$):

$$A_{mi} = \begin{cases} \frac{i(m-1)}{N} - 1, & i=1 \\ \frac{m-1}{N} i^{i-1}, & i=2, \dots, N \end{cases}$$

$$B_{mi} = \begin{cases} 0, & i=1 \\ i(i-1) - 1, & i=2 \\ \frac{m-1}{N} i^{i-2}, & i=3, \dots, N \end{cases}$$

Results and discussion

For the established piecewise linear HBIM and $\beta = 1$, tab. 2 lists estimates to α [$\sim(a_1/2)^{1/2}$], temperature v at $x = s/2$, incident heat flux, and s . The results converge at the expected rate $O(n^{-1})$ [14]. Table 3 shows the same four parameters computed using the three high-order methods, for various values of N . The methods give the expected very similar results to the parameter estimates listed, converging rapidly with N . For $N = 5$ the results are one to two orders of magnitude better than the piecewise-linear approach with $n = 40$ (8 times as many equations), and conform to the quadratic form for $N = 2$. Collocation is marginally worse due to the pointwise (as opposed to element-based) nature of the established balance (in this case forcing the residual to zero). The high-order methods provide very similar values for the coefficients a_i , shown in tab. 4, that are consistent with the data in tab. 3. Column-by-column the a_i converge rapidly with N , in particular $a_1 \sim 2\alpha^2$.

Table 2. Melt parameter α^* , temperature $v(x = s/2)$, incident heat flux $v'(x = 0)$, and melt front s , at $t = 1$, using a piecewise linear approximant

n	α^*	v	v'/x	s
10	0.6139	0.4575	-0.9038	1.2279
20	0.6170	0.4552	-0.9072	1.2339
40	0.6185	0.4540	-0.9090	1.2370
Exact	0.6201	0.4528	-0.9108	1.2401

Table 3. Melt parameter α^* , temperature $v(x = s/2)$, incident heat flux $v'(x = 0)$, and melt front s , at $t = 1$, using high-order polynomials

	N	α^*	v	$\partial v/\partial x$	s
Sub-division	2	0.6365	0.4526	-0.9346	1.2730
	3	0.6197	0.4549	-0.9108	1.2393
	4	0.6200	0.4528	-0.9107	1.2400
	5	0.6201	0.4528	-0.9108	1.2401
Galerkin	2	0.6365	0.4526	-0.9346	1.2730
	3	0.6198	0.4549	-0.9111	1.2396
	4	0.6201	0.4529	-0.9108	1.2401
	5	0.6201	0.4529	-0.9108	1.2401
Collocation	2	0.6325	0.4500	-0.9487	1.2649
	3	0.6159	0.4528	-0.9227	1.2318
	4	0.6198	0.4529	-0.9097	1.2395
	5	0.6202	0.4528	-0.9104	1.2403
	Exact	0.6201	0.4528	-0.9108	1.2401

Table 4. Coefficients a_i for sub-division, Galerkin, and collocation

	N	a_1	a_2	a_3	a_4	a_5	a_6	a_7
Sub-division	2	0.81025	0.18975					
	3	0.76794	0.33530	-0.10324				
	4	0.76882	0.29949	-0.03470	-0.03361			
	5	0.76896	0.29438	-0.01583	-0.05681	0.00930		
	6	0.76896	0.29559	-0.02238	-0.04324	-0.00230	0.00407	
	7	0.76896	0.29567	-0.02300	-0.04131	-0.00593	0.00625	-0.00063
Galerkin	2	0.81025	0.18975					
	3	0.76832	0.33400	-0.10232				
	4	0.76894	0.29949	-0.03526	-0.03317			
	5	0.76896	0.29472	-0.01659	-0.05628	0.00919		
	6	0.76896	0.29560	-0.02241	-0.04329	-0.00287	0.00401	
	7	0.76896	0.29566	-0.02293	-0.04147	-0.00577	0.00618	-0.00062
Collocation	2	0.80000	0.20000					
	3	0.75864	0.34611	-0.10475				
	4	0.76819	0.30132	-0.03484	-0.03468			
	5	0.76923	0.29312	-0.01374	-0.05803	0.00943		
	6	0.76897	0.29552	-0.02226	-0.04327	-0.00310	0.00415	
	7	0.76895	0.29571	-0.02315	-0.04105	-0.00616	0.00633	-0.00063

A familiar characteristic of high-order polynomial approximants is their tendency to oscillate and thereby introduce spurious (numerical) artifacts into the solution profile. Figures 4 and 5 show the spatial \log_{10} |relative error| distribution for values of N using the three high-order schemes. This broadly indicates the number of digits of accuracy at each node x_i . Approximately one digit of accuracy is gained with each order of the approximant, with the Galerkin approach giving slightly better accuracy than the sub-division approach for high values of N . For odd orders ($N = 3, 5, 7,$ and 9 are shown), sub-division (fig. 4) maintains a (desirable) smoother spatial error distribution.

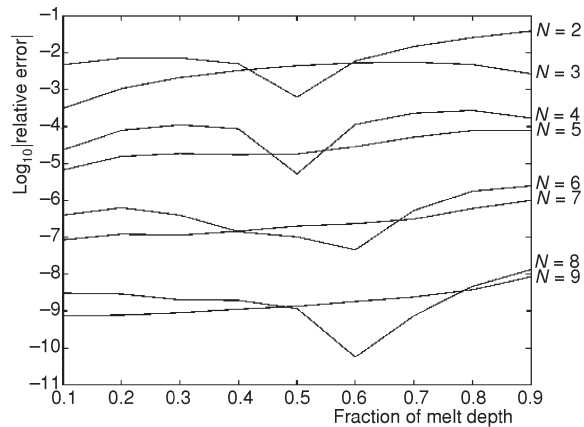


Figure 4. \log_{10} |error| profiles at $t = 1$ (sub-division)

Establishing elemental heat balances appears to counteract the natural tendency of high-order polynomial approximants to oscillate due to a naturally increasing number of turning points. In other words, sub-division maintains the correct shape and resists the introduction numerical artifacts into the solution that have no physical meaning.

Figure 6 shows the observed relative error (including the sign) for each of the three high-order formulations across the solution domain. The formulations exhibit fairly distinct error profiles and across a range of orders, N , it is not easy to identify one particularly dominant method. Table 5 lists the mean $\log|error|$ and standard deviation (SD) for the error profiles shown in fig. 6.

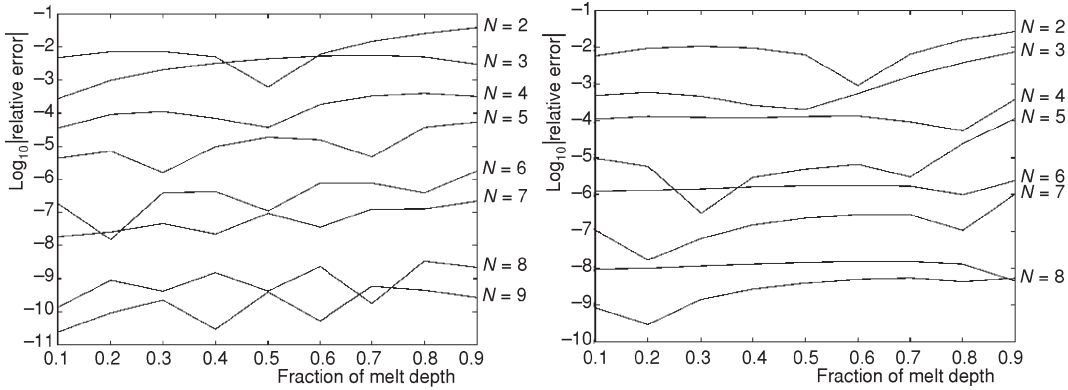


Figure 5. $\log_{10}|\text{error}|$ profiles at $t = 1$; (a) Galerkin, (b) collocation

The bold values indicate the best approach for each specified value of N , showing a mid-range dominance by Galerkin, with spatial sub-division emerging as machine precision is approached – the Galerkin system of non-linear equations becomes increasingly ill-conditioned.

However, for all listed orders, N , the standard deviation of Galerkin is highest, (crudely) indicating a wider “spread” of precision across the solution domain. For $N = 6$ and $N = 10$, collocation provides remarkably consistent precision.

Table 5. Mean and standard deviation of data presented in fig. 6

N	Sub-division		Galerkin		Collocation	
	Mean	SD	Mean	SD	Mean	SD
2	-2.13	0.52	-2.13	0.52	-2.12	0.41
3	-2.60	0.41	-2.60	0.44	-3.08	0.53
4	-4.10	0.54	-3.90	0.40	-3.90	0.22
5	-4.58	0.36	-4.98	0.48	-5.21	0.70
6	-6.42	0.56	-6.52	0.60	-5.81	0.11
7	-6.65	0.36	-7.25	0.39	-6.83	0.50
8	-8.78	0.66	-9.12	0.51	-7.96	0.16
9	-8.78	0.35	-9.86	0.53	-8.63	0.44
10	-11.03	0.23	-11.77	0.37	-10.32	0.08
11	-10.96	0.35	-12.05	0.38	-10.67	0.48
12	-13.04	0.29	-12.13	0.43	-12.73	0.54
13	-13.20	0.35	-11.83	0.49	-12.65	0.50

Both mean and SD provide spatially-transparent measures of tendency and variation. Figure 7 displays the variation in slope (first difference) of the $\log|\text{error}|$. At this point it is clear that the Galerkin response is spatially more oscillatory and, except for $N = 2, 4, 6,$ and 8 , sub-division shows a considerably more moderate fluctuation (that even betters that of collocation). It is a fairly subjective analysis but the indication from these crude tools is that spatial sub-division smoothes the behaviour of the error, thus leading to more consistency in accuracy across the solution domain.

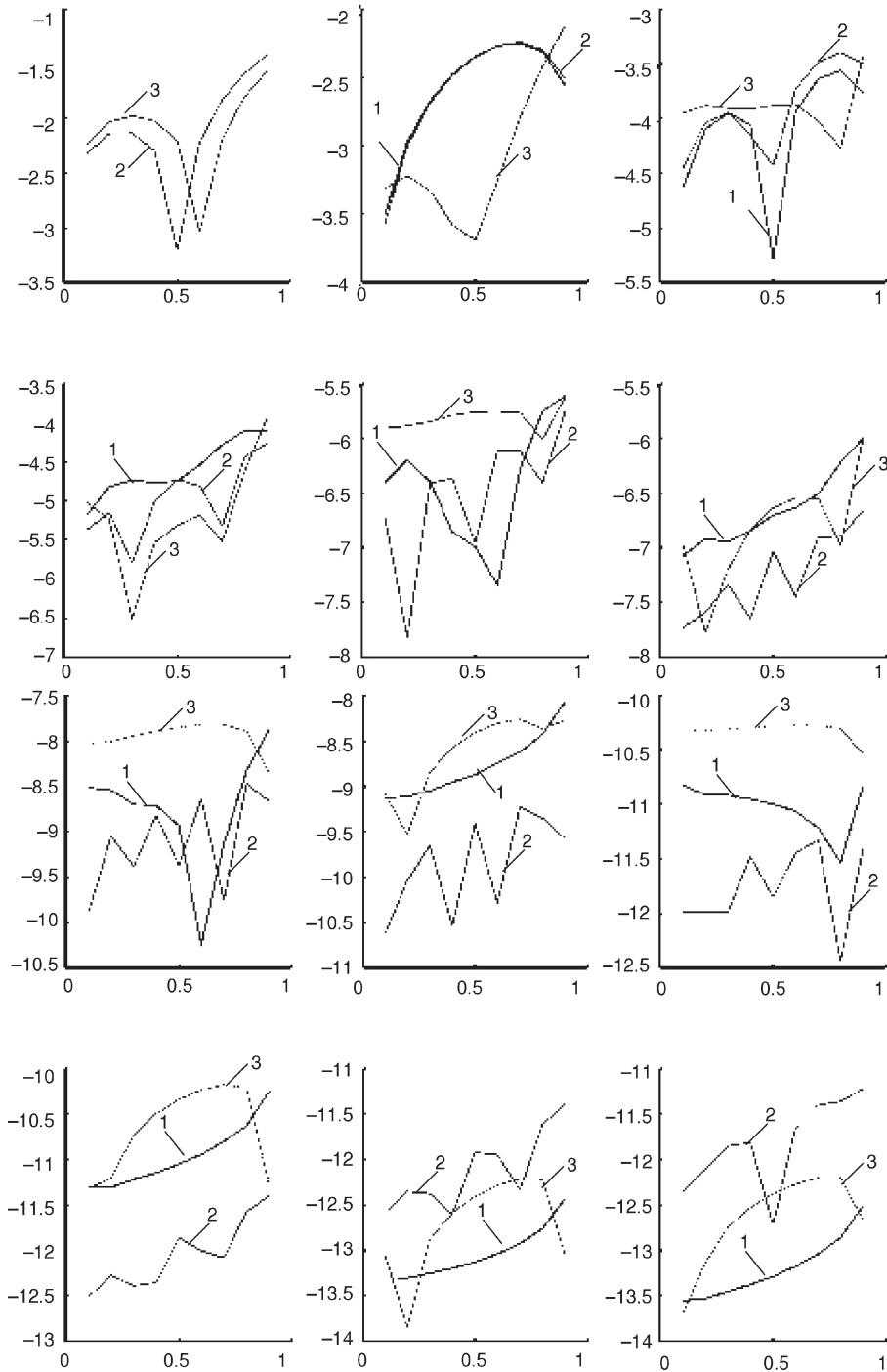


Figure 6. Orders $N=2$ to 13; $e = \log_{10}|\text{error}|$ spatial distribution for 1 – blue sub-division, 2 – red Galerkin, and 3 – green collocation (color image see on our web site)

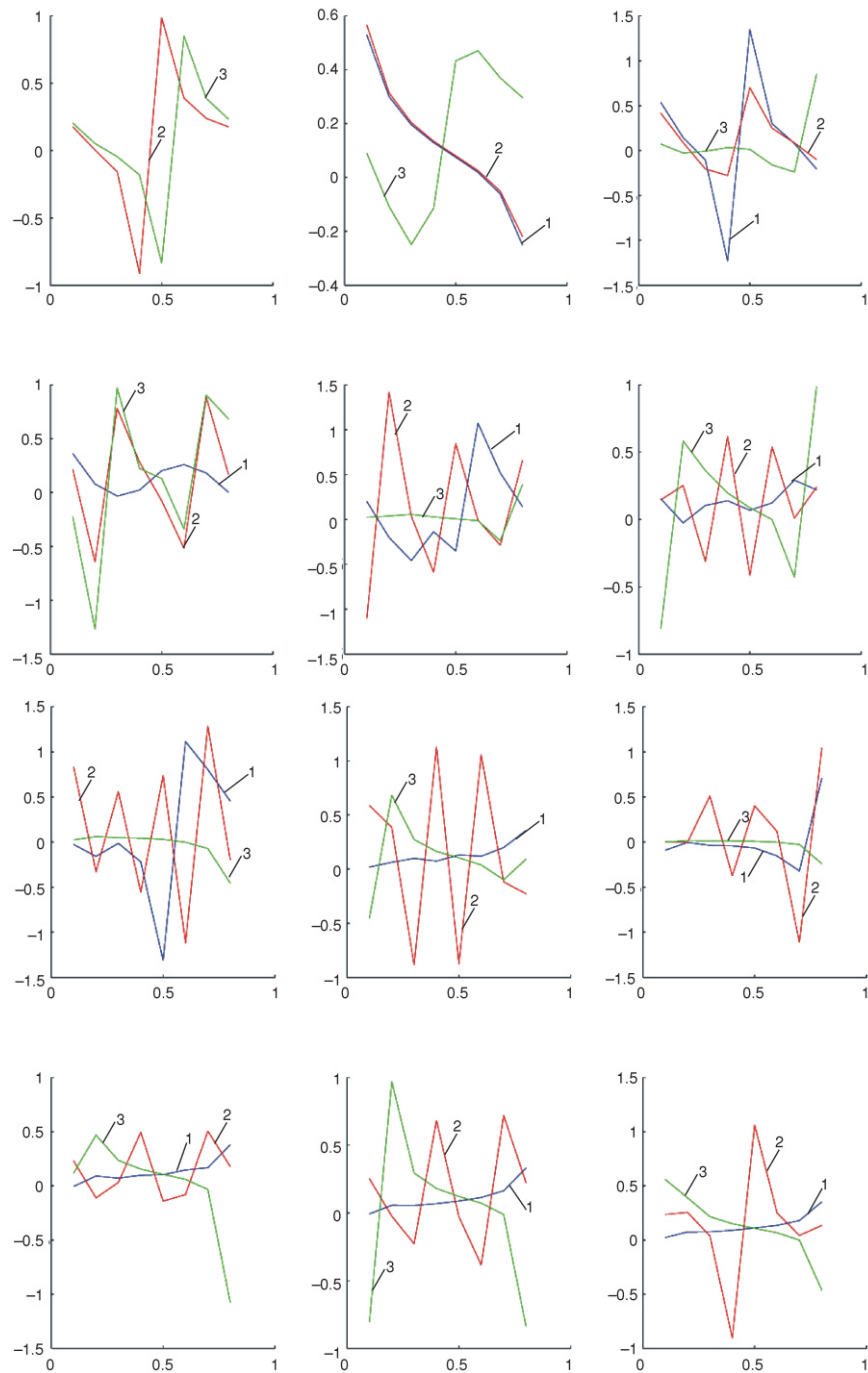


Figure 7. Orders $N = 2$ to 13; spatial distribution of Δe , $e = \log_{10}|\text{error}|$ for 1 – blue sub-division, 2 – red Galerkin, and 3 – green collocation (color image see on our web site)

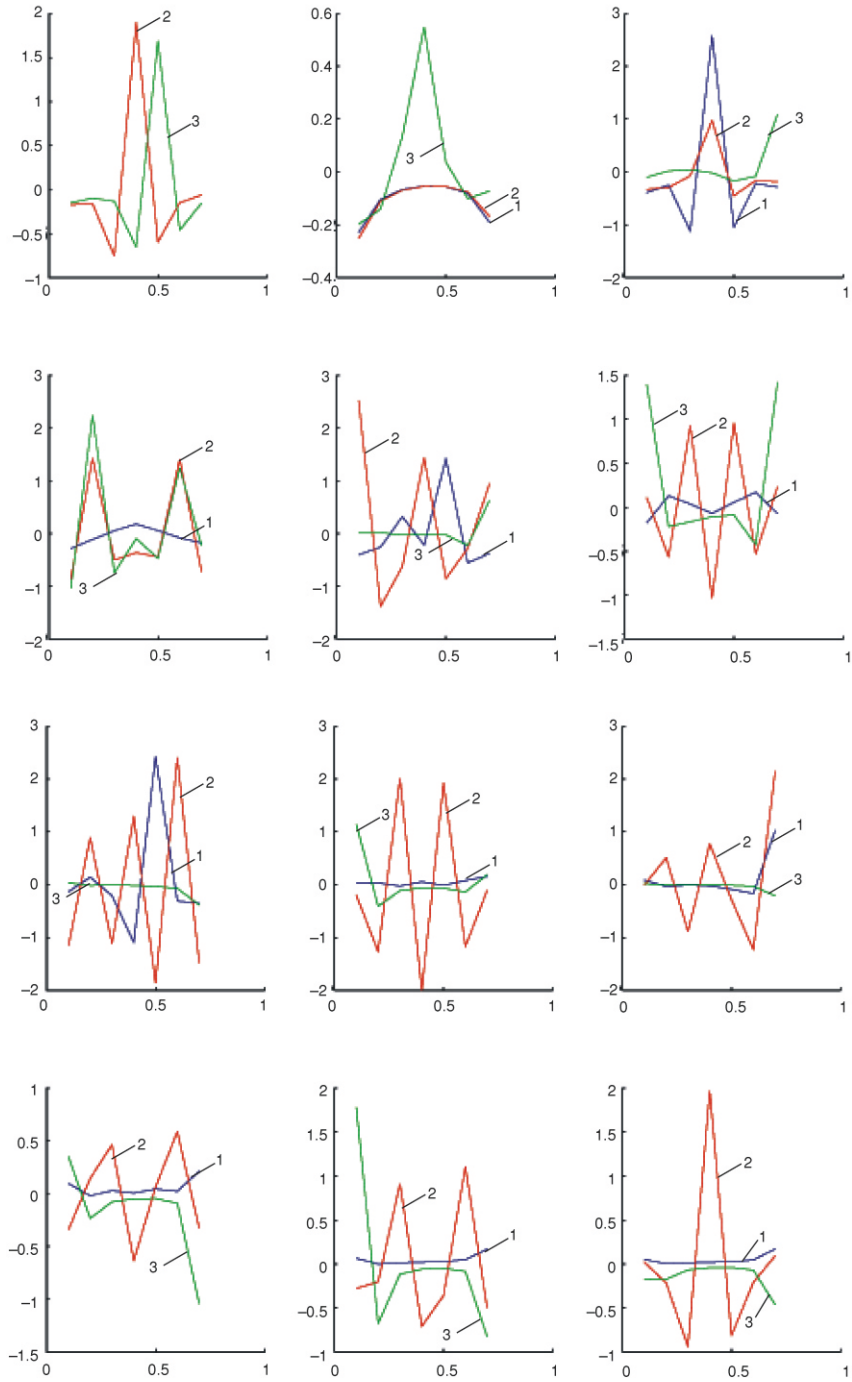


Figure 8. Orders $N = 2$ to 13; spatial distribution of $\Delta^2 e$, $e = \log_{10}|\text{error}|$ for 1 – blue sub-division, 2 – red Galerkin, and 3 – green collocation (color image see on our web site)

- [12] Bell, G. E., The Prediction of Frost Penetration, *Int. J. Numer. Anal. Meths. Geomechanics*, 6 (1982), 2, pp. 287-290
- [13] Bell, G. E., Abbas, S. K., Convergence Properties of the Heat Balance Integral Method, *Numer. Heat Transfer*, 8 (1985), 3, pp. 373-382
- [14] Mosally, F., Wood, A. S., Al-Fhaid, A., On the Convergence of the Heat Balance Integral Method, *Appl. Math. Mod.*, 29 (2005), 10, pp. 903-912
- [15] Caldwell, C., Chiu, C. K., Numerical Solution of Melting/Solidification Problems in Cylindrical Geometry, *Engineering Comp.*, 11 (1994), 4, pp. 357-363
- [16] Caldwell, J., Chan C-C., Spherical Solidification by the Enthalpy Method and the Heat Balance Integral Method, *Appl. Math. Mod.*, 24 (2000), 1, pp. 45-53
- [17] Caldwell, J., Kwan, Y. Y., Spherical Solidification by the Enthalpy Method and Heat Balance Integral Method, in: *Advanced Computational Methods in Heat Transfer VII* (Eds., B. Sunden, C. A. Brebbia), WIT, UK, 2002, pp. 532-541
- [18] Caldwell, C., Chiu, C. K., Numerical Solution of One-Phase Stefan Problems by the Heat Balance Integral Method, Part I – cylindrical and spherical geometries, *Comms. Numer. Meth. Engng.*, 16 (2000), 8, pp. 569-583
- [19] Wood, A. S., A New Look at the Heat Balance Integral Method, *Appl. Math. Mod.*, 25 (2001), 10, pp. 815-824

Authors' affiliations:

A. S. Wood (**corresponding author**)

School of Engineering, Design and Technology, EDT1

University of Bradford

Bradford West, Yorkshire BD7 1DP

United Kingdom

E-mail: a.s.wood@bradford.ac.uk

F. Mosally, A. Al-Fhaid

Department of Mathematics,

King Abdulaziz University

Jeddah, Saudi Arabia

Paper submitted: May 27, 2008

Paper revised: June 10, 2008

Paper accepted: June 10, 2008